CrossMark

ORIGINAL PAPER: NANO- AND MACROPOROUS MATERIALS (AEROGELS, XEROGELS, CRYOGELS, ETC.)
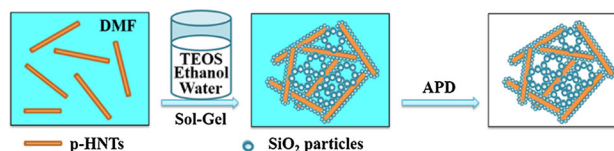
Novel three-dimensional halloysite nanotubes/silica composite aerogels with enhanced mechanical strength and low thermal conductivity prepared at ambient pressure

Hongli Liu[1,2] · Peng Chu[1,2] · Hongyan Li[1,2] · Haiyuan Zhang[1,2] · Jiadong Li[1,2]

Abstract Novel three-dimensional halloysite nanotubes (HNTs)/silica composite aerogels were fabricated to strengthen the nanostructure and overcome inherent fragility of silica aerogel by a sol–gel method using tetraethyl orthosilicate (TEOS) and 1,4-Phenylene diisocyanate (PPDI)-modified HNTs (p-HNTs) as the main materials, followed by an environmentally friendly ambient pressure drying (APD). The modification and dispersion of HNTs were investigated by using FTIR, SEM, TEM. Meanwhile, the morphology, mechanical properties, and thermal conductivity of aerogels were also studied. The results showed that the p-HNTs were uniformly dispersed in the silica aerogel. This resulted in composites with unique interpenetrating network microstructure that could give an enhanced mechanical properties to aerogels. The compressive strength was found to vary from 400 kPa to 1.45 MPa and thermal conductivity from 0.025 to 0.038 W/m K. In addition, randomly oriented p-HNTs can obviously reduce both the linear shrinkage and density of composite aerogels. The composites with outstanding properties prepared by APD are potential for building applications.

Graphical Abstract

1 Introduction

Silica aerogels have attracted the attention of many researchers because of their fascinating properties such as extremely low bulk density, remarkably low thermal conductivity, high porosity, and high surface area, which make it a promising candidate for various applications [1–5]. However, the inherent fragility and hygroscopic nature somewhat restrict their further applications [6, 7]. In addition, aerogels are normally synthesized by traditional supercritical drying method [8]. Hence, using a less expensive source and a simple drying operation in silica aerogels with improved mechanical properties is also highly desirable, which can make them used in more widespread practical applications.

To improve the mechanical properties of silica aerogels, many researchers have been working on various strategies. One of the promising ways is organic–inorganic hybridization. For instance, polyuria [9, 10], isocyanate [11–13], polystyrene [14, 15], polyurethane [16, 17], and polyimide [18–20] were used to improve the mechanical properties of silica gels by forming polymer conformal coatings over the silica skeletal structure to enhance the

✉ Hongli Liu
liuhonglitianjin@163.com

1   Tianjin Key Laboratory of Soft Soil Characteristics and Engineering Environment, Tianjin 300384, China

2   School of Materials Science and Engineering, Tianjin Chengjian University, Tianjin 300384, China

🖄 Springer

connection between the particles in these gels through a sol–gel hybrid process. These wet silica-polymer composite gels were then supercritically dried to obtain the final products, and it was observed that the mechanical strength of the aerogels could be greatly improved. This approach led to an increase in strength by up to a factor of 300 with only a 2–3-fold increase in density compared to unmodified aerogels [11, 21–23]. Considering the low thermal stability of the above-mentioned polymers, fibers are steadier in higher temperatures, have good chemical resistance and outstanding mechanical ability, and have quite a wide usage in many applications under high temperatures [24, 25]. Paramenter and Milstein in 1990s first modified silica aerogel with silica fibers, alumina fibers and aluminaborosilicate fibers with a relatively high mass density, which proved that applied fibers significantly increased the density of the created nanocomposites [26]. Yang et al. [27] used ceramic fiber as reinforcement, by sol–gel method and supercritical drying process to obtain silica aerogel composites with good mechanical properties. Yuan and coworkers prepared insulation composites using silica powder and glass fiber via press-forming method [28]. Due to the addition of glass fiber, the mechanical properties of the composites were improved, but the heat insulation performance decreased. However, Agnieszka et al. were the first to apply oxidizing modified carbon microfibers as silica aerogel component improved the adhesion between hydrophilic silica gel and the carbon material surface, which lowered the contraction of gel volume during its drying in atmospheric pressure and led to the more stable structure [29]. Much better parameters were achieved by Meador and coworkers while modifying silica aerogel with much lighter carbon nanofibers [30]. Drawbacks of hitherto solutions for this type of modification were the lack of fiber surface modification and a relatively high mass density of fibers leading to lack of chemical bonding between fibers and silica gel and increasing the thermal conductivity. In the case of this solution, an improvement of compressive strength by 5 % was achieved.

Halloysite nanotubes (HNTs) have a highly unusual meso/macroscopic superstructure with a well-defined nanotubular structure, which consists of outside-in alternate silica tetrahedron sheets and alumina octahedron sheets in a 1:1 stoichiometric ratio [31–33]. The length of the nanotubes was in the range of 0.2–1.5 μm. The interior diameter of the channels is about 10–35 nm, and the wall thickness is about 10–20 nm. According to previous reports, HNTs was evaluated as one-dimensional (1D) nanofillers for polymers. Many efforts have been devoted to the elaboration and study of mechanical and fire resistance properties of polymer/halloysite composites due to the environmentally friendly properties, low expense, good

mechanical and thermal stability of HNTs [34–37]. However, to the best of our best knowledge, the synthesis of HNTs/silica aerogel has not been reported clearly. Therefore, HNTs could be used as inexpensive alternatives to expensive carbon nanotubes (CNTs) or other nanomaterials for synthesizing HNTs/silica composite aerogels [38]. The exploration of novel 3D HNTs/silica structures for heat insulation application is necessary due to their expected superior performance. However, HNTs are polar nanomaterials which are easy to aggregates and can not be dispersed in matrix well, which would adversely affect the composite physical properties [39, 40]. Hence, HNTs would be modified in order to be laid up one-by-one and being isolated by a layer of matrix [41–43]. Surface modification may be conducted on HNTs via grafting or functionalization to enhance their adhesion [44].

In this work, novel HNTs/silica composite aerogels were fabricated by employing HNTs to intercalate silica aerogel network skeleton via directly ambient-drying HNTs/silica gel. HNTs are modified by 1,4-Phenylene diisocyanate (PPDI) to facilitate good interfacial interaction between the HNTs and silica. Functionalization of HNTs by PPDI, isocyanate groups improved its dispersion in the silica aerogel. Compared to the expensive and time-consuming supercritical drying process, the ambient-pressure drying (APD) process is less expensive and safer [45]. This amelioration simplifies the preparation method obviously and promotes the application of aerogels in building insulation. In this paper, we present a systematic study of the influence of different mass percentages of p-HNTs on the microstructure, mechanical and thermal properties, about which few reports have been published for HNTs/silica composite aerogels, and decrease the shrinkage that is often observed in monolithic aerogels during the drying process. The obtained composite aerogel had a relatively large specific surface area (526 m^2 g^{-1}), low thermal conductivity (0.025 W m^{-1} K^{-1} at 25 °C), and excellent mechanical properties, which are potential for building insulation applications.

2 Experimental section

2.1 Materials

Halloysite that is industrial grade was purchased from Zhejiang Fenghong Clay Co. (Zhejiang, China). Tetraethyl orthosilicate (TEOS), N, N-Dimethylformamide (DMF), methanol, and ethanol were purchased from Tianjin Fengchuan Chemical Reagent Science and Technology Co. Ltd. 1,4-Phenylene diisocyanate (PPDI) was purchased from Energy Chemical (Shanghai, China). Hydrochloric acid (HCl, 37 %) and aqueous ammonia (NH₃·H₂O, 38 %)

Fig. 1 Schematic illustration of the sol–gel and drying processes of the HNTs/silica composite aerogels
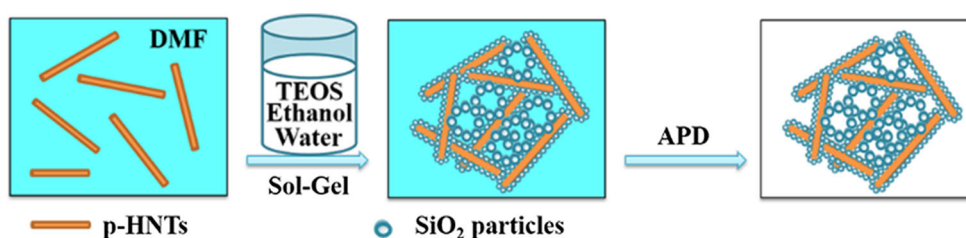
were received from provided by Tianjin Jiangtian Chemical Technology Co. Ltd. Solutions used in the study were prepared with deionized water. All of other chemicals were of analytical grade and used without further purification.

2.2 Functionalization of HNTs by PPDI

HNTs were treated three times with concentrated hydrochloric acid (HCl) (5 M), followed by methanol (CH_3OH) (99.8 %) and purified water. Coupling of PPDI onto the surface of HNT was carried out from its hydroxyl functional groups. First, HNT (2.50 g) was dispersed in 22.5 mL DMF and agitated for 2 h. Second, 2.5 g PPDI dissolved in 22.5 mL DMF was dropwised to HNTs solution stirring 5 min. Subsequently, put the mix solution into three-neck glass flask with magnetic rotor stirring at 65 °C for 2 h. The obtained suspension was cooled to room temperature and then centrifuged at 7000 rpm for 10 min. Purification was carried out in 60 mL toluene twice to remove the unreacted PPDI moieties. After drying in vacuum oven at 70 °C, 1.96 g p-HNTs (78.4 %) was obtained.

2.3 Preparation of modified HNTs/silica aerogel composites

Tetraethyl orthosilicate (TEOS) was used as a precursor of silica. Silica sols were prepared via a modified technique. Firstly, p-HNTs at different weight percentages (1.0, 3.0, 5.0 and 10 wt%) were dispersed in 10 ml of DMF (99.5 %) and then mixed in a solution containing 6 mL of TEOS, 10 ml of ethanol and 4 ml of water. The solution was initially stirred for 30 min and ultrasonicated for 60 min to inhibit any possible aggregation of p-HNTs. Subsequently, 0.07 ml of 35 % aqueous ammonia ($NH_3 \cdot H_2O$) was added into the TEOS/HNTs sol. The mixed sol was constantly stirred and then sonicated again for 20–30 min. The mixture was left to dry at 40 °C in atmospheric pressure for 4 days to remove the excess ethanol solvent. Figure 1 gives a schematic diagram for the sol–gel and drying processes of HNTs/silica composite aerogels. The dried mixtures were ground into dryer for further characterization. The aerogels with varied HNTs contents are noted as HSAX, and X (= 1.0, 3.0, 5.0, 10) is the weight percentage of

p-HNTs to silica aerogel (denoted as SA). As reference, silica sol–gel without p-HNTs was prepared in a similar approach.

2.4 Characterization

Fourier transform infrared (FTIR) spectroscopy was performed with Nicolet 380 FTIR Spectrometer in the wave number range of 4000–400 cm^{-1} to analyze the sample's molecular structure. The morphologies of the HNTs/silica aerogel composites were observed using scanning electron microscope (SEM, Hitachi S-4800), operated at an accelerating voltage of 10.0 kV, and a transmission electron microscope, TEM (JEOL 1011) operated at an accelerating voltage of 100 kV. The specific surface area and pore size distribution of the aerogels were commonly measured by the multipoint Brunauer–Emmett–Teller (BET) method on the basis of nitrogen adsorption–desorption isotherms at 77 K with a 3H-2000PS1 analysis instrument. The sample was degassed for at least 3 h at a temperature of 150 °C in vacuum in order to remove all the possible absorbed species. The thermal conductivity test of the aerogel and composite was performed by using a transient hot-wire method (TC3000E, XIA TECH, CHN), and the operating current range was 0–10 mA. The aerogel and composite sample were both rectangular (length × width × thickness correspond to 45 × 30 × 5 mm). Compression tests were carried out on a materials testing machine (CMT 6104 SANS, GER). The compressing speed was 6 mm min^{-1}, and the sample tested was a cylinder (diameter and height corresponds to 20 and 10 mm, respectively). The sample tested in the cyclic compression was the same as high strain compression and the load/unload speed was 5 mm min^{-1}.

3 Results and discussion

3.1 Characterizations of HNTs and p-HNTs

Figure 2 shows the SEM images of HNTs and p-HNTs. As shown in Fig. 2, the pristine HNTs tend to form aggregates in bundles. In contrast, the p-HNTs dispersed better. This could be due to the modification of PPDI that resulted in the reduction of van der Waals force and hydrogen-
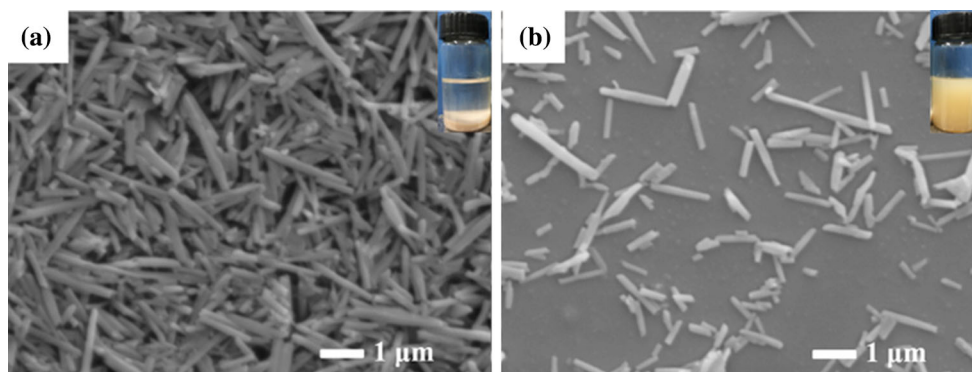
Fig. 2 SEM images of **a** pristine HNTs, **b** p-HNTs. The *insets* were the solutions of two kinds of HNTs: **a** raw HNTs dissolve in DMF; **b** p-HNTs (0.1 wt%) dissolved in DMF
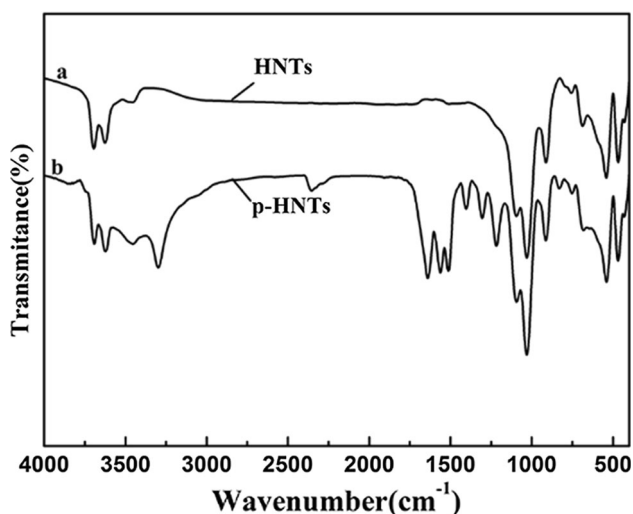
Fig. 3 FTIR spectra of HNTs and p-HNTs

bonding interactions among p-HNTs. The insets in Fig. 2 present the solubility of HNTs and p-HNTs dissolved in DMF. HNTs with a large amount of hydroxyl group are a polar mineral, and a well dispersion of them in organic solvents is difficult. The p-HNT with benzene groups makes it more easily dispersed in DMF.

Figure 3 shows the FTIR spectra of HNTs and p-HNTs. The double peaks at 3692 and 3623 cm^{-1} were ascribed to the stretching vibrations of Al–OH groups at the surface of HNTs [33]. The well peaks that appeared at ~ 685 cm^{-1} corresponded to the strongly polarized Si–O symmetric stretch. The peaks observed at ~ 762 cm^{-1} indicated the characteristics of the symmetric Si–O–Si stretch, in which the oxygen atoms moved at a right angle to the Si–Si lines and in the Si–O–Si planes, while the peak that appeared at ~ 1069 cm^{-1} was due to the characteristics of the Si–O–Si asymmetric stretch. The peak at 912 cm^{-1} was attributed to the bending vibration of Al–OH [46, 47]. In the case of HNTs-modified PPDI as shown in Fig. 3b, the peak

at 2270 cm^{-1} was attributed to the bending vibration of N=C=O. The characteristic peaks of benzene at 1600, 1503 cm^{-1} appeared, compared with HNTs. Apart from this, the peaks at about 1545 and 1649 cm^{-1} were characteristic vibrations of C=C and N–H, respectively. Namely, all of these observations indicated that HNTs have been modified successfully.

3.2 Morphological and structural characterizations of composite aerogels

Figure 4a is a scanning electron microscopy (SEM) image of unreinforced silica aerogel. The morphology of the unreinforced silica aerogel with disordered porous nanostructure can be observed in Fig. 4a, and a typical "pearl chain" of crosslinked and high-porosity skeleton network of aerogel were also shown.

As shown in Fig. 4b and c, the SEM image of HNTs/silica composite aerogel, a novel 3D porous structure composed of homogeneous p-HNTs and continuous silica aerogel structure can be found. It shows that these nanotubes exhibited good dispersion in the silica composite aerogel. Compared with the unreinforced silica aerogel without p-HNTs, more silica nanoparticles and more connecting points between the nanoparticles were formed in the same space. Consequently, the silica gel skeleton was stronger to withstand the shrinkage caused from the APD modification process. Meantime, the existence of nanofiber improved mechanical properties of the composite aerogel.

Figure 5 shows the TEM images of the silica aerogel and HNTs/silica composite aerogels. As shown in Fig. 5a, the framework of the unreinforced aerogels was made up of homogeneous nanoparticle networks, and no obvious aggregation domains. The TEM images of HNTs/silica composite aerogels HSA1.0, HSA3.0, and HSA10 were shown in Fig. 5b, c, d. It can be seen clearly that the
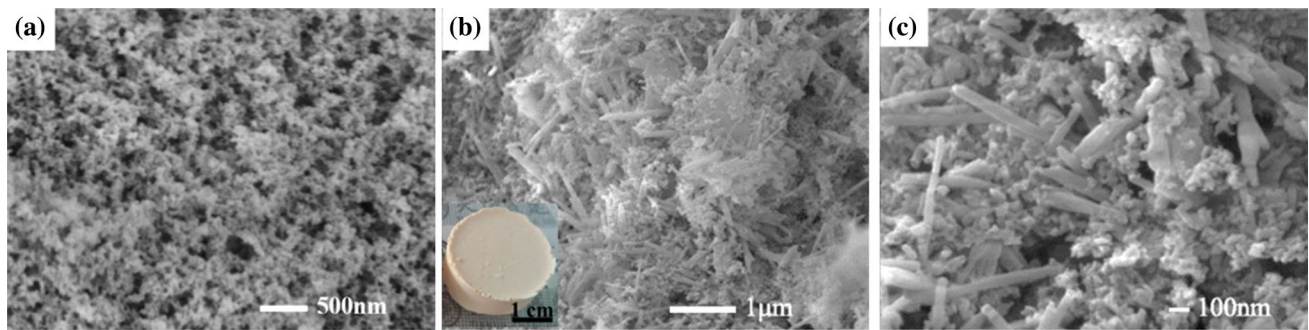
Fig. 4 SEM images of the surface morphologies: **a** unreinforced silica aerogel; **b** and **c** 10 wt% HNTs/silica composite aerogel. *Inset* in **b** is a photograph of HSA10
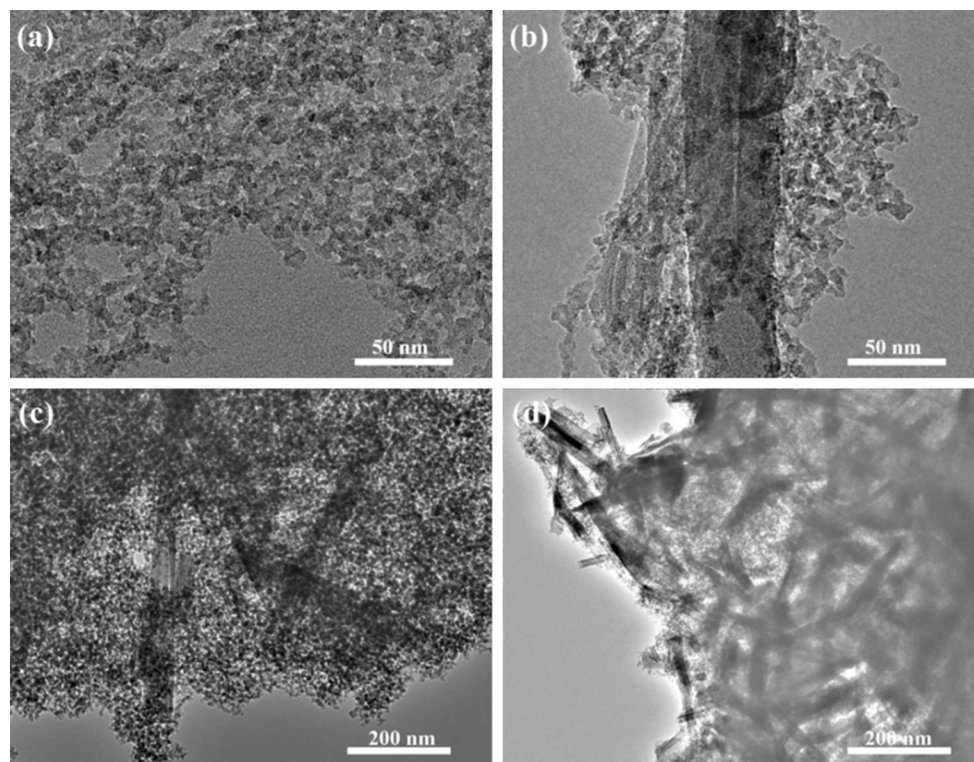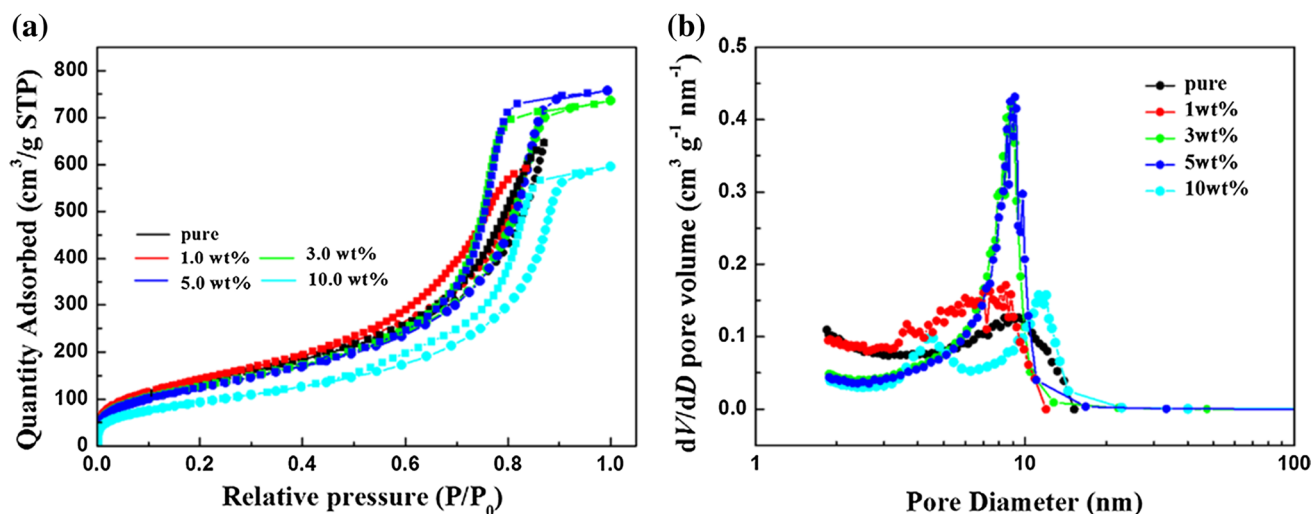

Fig. 5 TEM images of the HNTs/silica composite aerogels with various wt% of p-HNTs **a** 0; **b** 1; **c** 3; **d** 10

p-HNTs are uniformly dispersed in the silica framework. At higher wt% of p-HNTs, the aerogel composite framework (Fig. 5d) showed a porous 3D network composed of randomly oriented p-HNTs structures and silica networks. Although the sample was processed with ultrasonic treatment, the p-HNTs dispersed well in the silica network, which indicates the existence of strong interactions between the p-HNTs and silica nanoparticle networks caused by the condensation polymerization of TEOS. The TEM images confirmed that the 3D network of nanofibers were inlaid in the silica gel skeleton to form the interpenetrating network structure more effectively, for which the final compressive strength was up to 1.45 MPa. The

results were in good agreement with the previous SEM results.

3.3 N$_2$-sorption studies

To further determine the pore structure of aerogels, N$_2$ adsorption–desorption measurements were employed. Figure 6 illustrated N$_2$ adsorption/desorption isotherms and pore size of the HNTs/silica composite aerogels. As shown in Fig. 6a, all of the isotherms showed a typical type IV hysteresis loop as defined by IUPAC, which was characteristic of mesoporous materials [48]. The temporary locking of liquid N$_2$ and the delayed evaporation in the

(a)

(b)

Fig. 6 N_2 adsorption/desorption isotherms (**a**) and pore size (**b**) of the HNTs/silica composite aerogels

Table 1 Physical characteristics of the HNTs/silica composite aerogels after drying

Sample	Linear shrinkage	Density (g cm^{-3})	Specific surface area (m^2/g)	Average pore diameter(nm)	Pore volume (cm^3/g)
SA	–	0.20	509	6.23	1.15
HSA1.0	30 %	0.18	526	5.43	1.08
HSA3.0	25 %	0.17	472	6.86	1.31
HSA5.0	18 %	0.14	465	7.13	1.36
HSA10	14 %	0.12	346	7.50	1.04

desorption isotherm indicated that the product behaves similarly to the type H_3 hysteresis loops, implying the abundant presence of hierarchical pores. The hysteresis loop which appears at lower relative pressure (0.4–0.8) indicated the presence of mesopores and that at higher relative pressure (0.8–1.0) was attributed to macropores [49]. It was proposed that adsorption occurs on the surface of the silica aerogels and HNTs, which were overlayered with each other and constitute lots of pores contributing to the hysteresis loops. The pore distribution obtained using the Barrett–Joyner–Halenda (BJH) theory indicated the porosity characteristics of HNTs/silica aerogels (Fig. 6b). It can be seen that the aerogels show a hierarchical porous structure, and moreover, the introduction of p-HNTs can increase the percentage of mesopores, which was beneficial to prevent heat transfer. The N_2 adsorption–desorption results were in good agreement with the SEM observations. The specific surface areas, pore volumes and mean pore diameters of all samples are shown in Table 1. It can be seen that 1.0 wt% HNTs/silica aerogels exhibited the largest surface area (526 m^2 g^{-1}) much higher than that of silica aerogel (509 m^2 g^{-1}). The reason could be that 1D p-HNTs were uniformly dispersed in the silica aerogel, which resulted in composites with unique interpenetrating network microstructure that will in turn produce more

mesopores, larger specific surface area and lower density. It should also be noted that the specific surface area decreases with further increase in p-HNTs content, which could be caused by the aggregate of p-HNTs destroying the network structure of the aerogel to decrease the exposed surface area [50].

3.4 Mechanical and thermal properties of composite aerogels

The effects of adding p-HNTs to strengthen aerogels were evaluated from sample stress–strain curves shown in Fig. 7. The strength of the HNTs/silica aerogel composites increases with the content of the p-HNTs. It is apparent that the addition of the nanotubes did not increase the density, and thus the increase in the compressive stress could be attributed to the 3D structure of halloysite nanotubes with the specific strength and stiffness, and the increased connectivity within the microstructure which was able to transfer the load more effectively. Moreover, the mechanical behavior improvement was noticeable from the much higher energy that the aerogel composite was able to absorb up to the maximum compression strength.

According to the previous results, the unmodified silica aerogels failed at 5–10 % compressive strain and showed
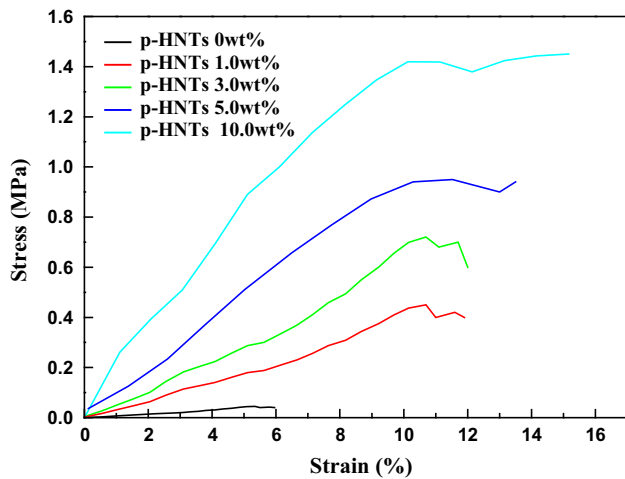
Fig. 7 Stress strain curves of different reinforced aerogels

compressive strength of 0.04 MPa. The compressive strength was higher for aerogels modified with greater than 3 wt% p-HNTs (Fig. 8a). A 36-fold increase in compressive strength compared to unmodified aerogel was obtained for aerogels modified with 10 wt% p-HNTs. The increase in p-HNTs content in aerogel could be a contributing factor to higher compressive strength. As is evident, these dependences were relatively weak and could not account for large increases reported in Fig. 8a. The p-HNTs were uniformly dispersed in the silica aerogel, which resulted in composites with unique interpenetrating network microstructure that could offer excellent mechanical properties to aerogels as supported by the SEM discussed earlier accounts for such large increases in compressive strength. The inset in Fig. 8a is the SEM image of failed/deformed samples (10 wt%) from compression tests. It can be noticed that the 3D structure of halloysite nanotubes

transfers to 2D structure under compression and the deformation leading to the collapse of the aerogel composite. The thermal conductivity of aerogels strongly depends on the number of network connecting points and on the applied mass to reinforce them [25]. Thus, with the increase of p-HNTs content, thermal conductivity of the composite aerogels increased (Fig. 8b). The p-HNTs as an inorganic nanomaterial, to a certain extent, increase thermal conductivity of the composite aerogels, but the small rate of increase could be due to its unique network structure.

3.5 Shrinkage and density of composite aerogels

Furthermore, the physical properties of the samples including the density, the specific surface area and the linear shrinkage ratio from wet gels to the aerogels are summarized in Table 1. The densities of the aerogel composites in the range of 0.20–0.12 g cm^{-3} increased with the augment of the weight percentage (0–10 %) of p-HNTs, while the linear shrinkage decreased from 30 to 14 %. The shrinkage mostly occurs in the process of ambient pressure drying, resulting from capillary force caused by the interaction between the solvent and the skeleton of the gels [51]. Two factors could be taken into account to explain the significant decrease in aerogel shrinkage: (i) randomly oriented p-HNTs structures could lead to the pore size increase and the capillary pressure reduction inside the matrix of aerogels; (ii) according to the excellent mechanical strength and dispersibility, as well as the strong interaction with the silica matrix, randomly oriented HNTs could significantly reinforce the network of gels and improve the resistance to collapse during the ambient pressure drying process.
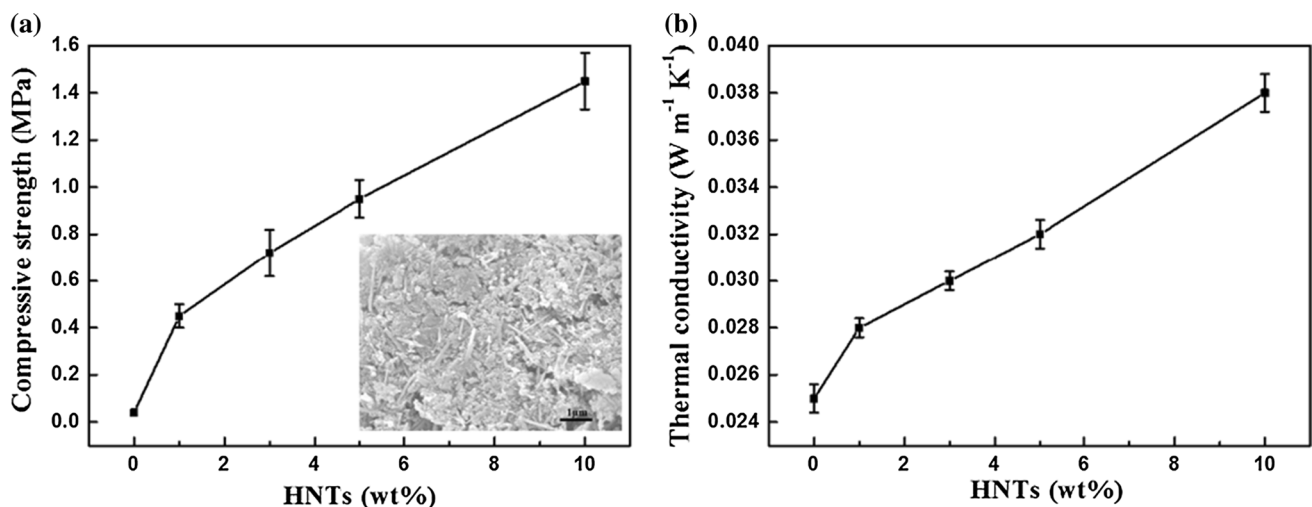

Fig. 8 Compressive strength (**a**) and thermal conductivity (**b**) of composite aerogels as a function of p-HNTs content. The *inset* in **a** is the SEM image of failed/deformed samples (10 wt%) from compression tests

4 Conclusions

In summary, a facile, efficient, and environmentally friendly strategy was utilized to fabricate novel 3D HNTs/silica aerogels, with linear shrinkage that decreased from 30 to 14 % as the thermal conductivity of the aerogels increased from 0.025 to 0.038 W/m K. The p-HNTs were uniformly dispersed in the silica aerogel, which resulted in composites with unique interpenetrating network that could finally lead to the more stable aerogel nanostructure. Moreover, the existence of strong interactions between the p-HNTs and silica nanoparticle networks strengthened the silica aerogel frame leading to high compressive strength as high as 1.45 MPa. The obtained aerogel composites prepared by APD had a relatively low cost, low thermal conductivity, and excellent mechanical properties, making them suitable for use as an thermal insulation for building applications.

References

1. Kistler S (1931) Coherent expanded aerogels and jellies. Nature 127:741
2. Yun S, Luo H, Gao Y (2015) Low-density, hydrophobic, highly flexible ambient-pressure-dried monolithic bridged silsesquioxane aerogels. J Mater Chem A 3:3390–3398
3. Guo H, Meador MA, McCorkle L, Quade DJ, Guo J, Hamilton B, Cakmak M, Sprowl G (2011) Polyimide aerogels cross-linked through amine functionalized polyoligomeric silsesquioxane. ACS Appl Mater Interfaces 3(2):546–552
4. Gibiat V, Lefeuvre O, Woignier T, Pelous J, Phalippou J (1995) Acoustic properties and potential applications of silica aerogels. J Non-Cryst Solids 186:244–255
5. Ihara T, Gao T, Grynning S, Jelle BP, Gustavsen A (2015) Aerogel granulate glazing facades and their application potential from an energy saving perspective. Appl Energy 142:179–191
6. Gao T, Jelle BP, Sandberg LIC, Gustavsen A (2013) Monodisperse hollow silica nanospheres for nano insulation materials: synthesis, characterization, and life cycle assessment. ACS Appl Mater Interfaces 5(3):761–767
7. ElKhatat AM, Al-Muhtaseb SA (2011) Advances in tailoring resorcinol-formaldehyde organic and carbon gels. Adv Mater 23(26):2887–2903
8. Hu X, Zheng S, Zhu L, Tanyi AR, Lan H et al (2013) Adsorption of 2-phenylethyl alcohol on silica aerogel from saturated solution in supercritical CO_2. J Supercrit Fluids 79:41–45
9. Sabri F, Leventis N, Hoskins J, Schuerger AC, Sinden-Redding M, Britt D, Duran RA (2011) Spectroscopic evaluation of polyurea crosslinked aerogels, as a substitute for RTV-based chromatic calibration targets for spacecraft. Adv Space Res 47(3):419–427
10. Sabri F, Marchetta J, Smith KM (2013) Thermal conductivity studies of a polyurea cross-linked silica aerogel-RTV 655

11. compound for cryogenic propellant tank applications in space. Acta Astronaut 91:173–179
11. Leventis N, Sotiriou-Leventis C, Zhang G, Rawashdeh A-MM (2002) Nanoengineering strong silica aerogels. Nano Lett 2(9):957–960
12. Meador MAB, Capadona LA, McCorkle L, Papadopoulos DS, Leventis N (2007) Structure-property relationships in porous 3D nanostructures as a function of preparation conditions: isocyanate cross-linked silica aerogels. Chem Mater 19(9):2247–2260
13. Nguyen BN, Meador MAB, Medoro A, Arendt V, Randall J, McCorkle L, Shonkwiler B (2010) Elastic behavior of methyltrimethoxysilane based aerogels reinforced with tri-isocyanate. ACS Appl Mater Interfaces 2(5):1430–1443
14. Wang X, Zhang H, Jana SC (2013) Sulfonated syndiotactic polystyrene aerogels: properties and applications. J Mater Chem A 1(44):13989
15. Zhang Y, Li H, Xu Z, Bu W, Liu C, Dong J, Hu Y (2014) Synthesis of low dispersity star-like polyethylene: a combination of click chemistry and a sol–gel process. Polym Chem 5(13):3963
16. Duan Y, Jana SC, Lama B, Espe MP (2013) Reinforcement of silica aerogels using silane-end-capped polyurethanes. Langmuir 29(20):6156–6165
17. Talebi Mazraeh-shahi Z, Mousavi Shoushtari A, Bahramian AR, Abdouss M (2015) Synthesis, pore structure and properties of polyurethane/silica hybrid aerogels dried at ambient pressure. J Ind Eng Chem 21:797–804
18. Guo H, Meador MA, McCorkle L, Quade DJ, Guo J, Hamilton B, Cakmak M, Sprowl G (2011) Polyimide aerogels cross-linked through amine functionalized polyoligomeric silsesquioxane. ACS Appl Mater Interfaces 3(2):546–552
19. Yan P, Zhou B, Du A (2014) Synthesis of polyimide cross-linked silica aerogels with good acoustic performance. RSC Adv 4(102):58252–58259
20. Zhang L, Wu J, Zhang X, Gong G, Liu J, Guo L (2015) Multifunctional, marvelous polyimide aerogels as highly efficient and recyclable sorbents. RSC Adv 5(17):12592–12596
21. Katti A, Shimpi N, Roy S, Lu H, Fabrizio EF, Dass A, Capadona LA, Leventis N (2006) Chemical, physical, and mechanical characterization of isocyanate cross-linked amine-modified silica aerogels. Chem Mater 18(2):285–296
22. Leventis N (2007) Three-dimensional core-shell superstructures: mechanically strong aerogels. Acc Chem Res 40(9):874–884
23. Nguyen BN, Meador MAB, Tousley ME, Shonkwiler B, McCorkle L, Scheiman DA, Palczer A (2009) Tailoring elastic properties of silica aerogels cross-linked with polystyrene. ACS Appl Mater Interfaces 1(3):621–630
24. Yi X, Zhang L, Wang F, Shen X, Cui S, Zhang J, Wang X (2014) Mechanically reinforced composite aerogel blocks by self-growing nanofibers. RSC Adv 4(89):48601–48605
25. Lu Z, Yuan Z, Liu Q, Hu Z, Xie F, Zhu M (2015) Multi-scale simulation of the tensile properties of fiber-reinforced silica aerogel composites. Mater Sci Eng, A 625:278–287
26. Parmenter KE, Milstein F (1998) Mechanical properties of silica aerogels. J Non-Cryst Solids 223(3):179–189
27. Yang X, Wei J, Shi D, Sun Y, Lv S, Feng J, Jiang Y (2014) Comparative investigation of creep behavior of ceramic fiber-reinforced alumina and silica aerogel. Mater Sci Eng A 609:125–130
28. Yuan B, Ding S, Wang D, Wang G, Li H (2012) Heat insulation properties of silica aerogel/glass fiber composites fabricated by press forming. Mater Lett 75:204–206
29. Ślosarczyk A, Wojciech S, Piotr Z, Paulina J (2015) Synthesis and characterization of carbon fiber/silica aerogel nanocomposites. J Non-Cryst Solids 416:1–3

30. Maleki H, Durães L, Portugal A (2014) An overview on silica aerogels synthesis and different mechanical reinforcing strategies. J Non-cryst Solids 385:55–74

31. Liu Y, Jiang X, Li B, Zhang X, Liu T, Yan X, Ding J, Cai Q, Zhang J (2014) Halloysite nanotubes@reduced graphene oxide composite for removal of dyes from water and as supercapacitors. J Mater Chem A 2(12):4264

32. Wang Q, Wang Y, Zhao Y, Zhang B, Niu Y, Xiang X, Chen R (2015) Fabricating roughened surfaces on halloysite nanotubes via alkali etching for deposition of high-efficiency Pt nanocatalysts. CrystEngComm 17(16):3110–3116

33. Zhou C, Sun T, Gao Q, Alshameri A, Zhu P, Wang H, Qiu X, Ma Y, Yan C (2014) Synthesis and characterization of ordered mesoporous aluminosilicate molecular sieve from natural halloysite. J Taiwan Inst Chem E 45(3):1073–1079

34. Vahedi V, Pasbakhsh P, Chai S-P (2015) Toward high performance epoxy/halloysite nanocomposites: new insights based on rheological, curing, and impact properties. Mater Des 68:42–53

35. Zhang Y, Pan J, Yan Y, Shi W, Yu L (2014) Synthesis and evaluation of stable polymeric solid acid based on halloysite nanotubes for conversion of one-pot cellulose to 5-hydroxymethylfurfural. RSC Adv 4(45):23797

36. Zeng S, Reyes C, Liu J, Rodgers PA, Wentworth SH, Sun L (2014) Facile hydroxylation of halloysite nanotubes for epoxy nanocomposite applications. Polymer 55(25):6519–6528

37. Liu M, Jia Z, Jia D, Zhou C (2014) Recent advance in research on halloysite nanotubes-polymer nanocomposite. Prog Polym Sci 39(8):1498–1525

38. Ding X, Wang H, Chen W, Liu J, Zhang Y (2014) Preparation and antibacterial activity of copper nanoparticle/halloysite nanotube nanocomposites via reverse atom transfer radical polymerization. RSC Adv 4(79):41993–41996

39. Luo Z, Wang A, Wang C, Qin W, Zhao N, Song H, Gao J (2014) Liquid crystalline phase behavior and fiber spinning of cellulose/ionic liquid/halloysite nanotubes dispersions. J Mater Chem A 2(20):7327–7336

40. Zhang L, Wang T, Liu P (2008) Polyaniline-coated halloysite nanotubes via in situ chemical polymerization. Appl Surf Sci 255(5):2091–2097

41. Liu M, Jia Z, Liu F, Jia D, Guo B (2010) Tailoring the wettability of polypropylene surfaces with halloysite nanotubes. J Colloid Interface Sci 350(1):186–193

42. Barrientos-Ramírez S, Oca-Ramírez GMd, Ramos-Fernández EV, Sepúlveda-Escribano A, Pastor-Blas MM, González-Montiel A (2011) Surface modification of natural halloysite clay nanotubes with aminosilanes. Application as catalyst supports in the atom transfer radical polymerization of methyl methacrylate. Appl Catal A 406(1):22–33

43. Rooj S, Das A, Heinrich G (2011) Tube-like natural halloysite/fluoroelastomer nanocomposites with simultaneous enhanced mechanical, dynamic mechanical and thermal properties. Eur Polym J 47(9):1746–1755

44. Kango S, Kalia S, Celli A, Njuguna J, Habibi Y, Kumar R (2013) Surface modification of inorganic nanoparticles for development of organic–inorganic nanocomposites—a review. Prog Polym Sci 38(8):1232–1261

45. Yun S, Luo H, Gao Y (2014) Ambient-pressure drying synthesis of large resorcinol-formaldehyde-reinforced silica aerogels with enhanced mechanical strength and superhydrophobicity. J Mater Chem A 2(35):14542–14549

46. Albdiry MT, Yousif BF (2014) Role of silanized halloysite nanotubes on structural, mechanical properties and fracture toughness of thermoset nanocomposites. Mater Des 57:279–288

47. Liu M, Zhang Y, Zhou C (2013) Nanocomposites of halloysite and polylactide. Appl Clay Sci 75:52–59

48. Wang H, Shi L, Yan T, Zhang J, Zhong Q, Zhang D (2014) Design of graphene-coated hollow mesoporous carbon spheres as high performance electrodes for capacitive deionization. J Mater Chem A 2(13):4739–4750

49. Xu X, Liu Y, Lu T, Sun Z, Chua DHC, Pan L (2015) Rational design and fabrication of graphene/carbon nanotubes hybrid sponge for high-performance capacitive deionization. J Mater Chem A 3:13418–13425

50. Yusof Y, Johan MR (2014) Concentration-dependent properties of amorphous carbon nanotube/silica composites via the sol–gel technique. CrystEngComm 16(36):8570–8575

51. Guo K, Song H, Chen X, Du X, Zhong L (2014) Graphene oxide as an anti-shrinkage additive for resorcinol-formaldehyde composite aerogels. Phys Chem Chem Phys 16(23):11603–11608